

## *Supporting Information*

Local charge-carrier dynamics of a particulate Ga-doped  $\text{La}_5\text{Ti}_2\text{Cu}_{0.9}\text{Ag}_{0.1}\text{O}_7\text{S}_5$  photocatalyst by pattern-illumination time-resolved phase microscopy and the impact of Rh cocatalyst

Tatsuya Chugenji,<sup>1</sup> Zhenhua Pan,<sup>1</sup> Vikas Nandal,<sup>2</sup> Kazuhiko Seki,<sup>2</sup> Kazunari Domen,<sup>3,4\*</sup> and Kenji Katayama<sup>1\*</sup>

<sup>1</sup> Department of Applied Chemistry, Chuo University, Tokyo 112-8551, Japan

<sup>2</sup> Global Zero Emission Research Center (GZR), National Institute of Advanced Industrial Science and Technology (AIST), Onogawa 16-1 AIST West, Tsukuba 305-8569, Japan

<sup>3</sup> Research Initiative for Supra-Materials, Interdisciplinary Cluster for Cutting Edge Research, Shinshu University, Nagano 380-8553, Japan

<sup>4</sup> Office of University Professors, The University of Tokyo, Tokyo 113-8656, Japan

\*Corresponding author

K. Katayama, Phone: +81-3-3817-1913, E-mail: [kkata@kc.chuo-u.ac.jp](mailto:kkata@kc.chuo-u.ac.jp)

K. Domen, E-mail: [domen@chemsys.t.u-tokyo.ac.jp](mailto:domen@chemsys.t.u-tokyo.ac.jp)

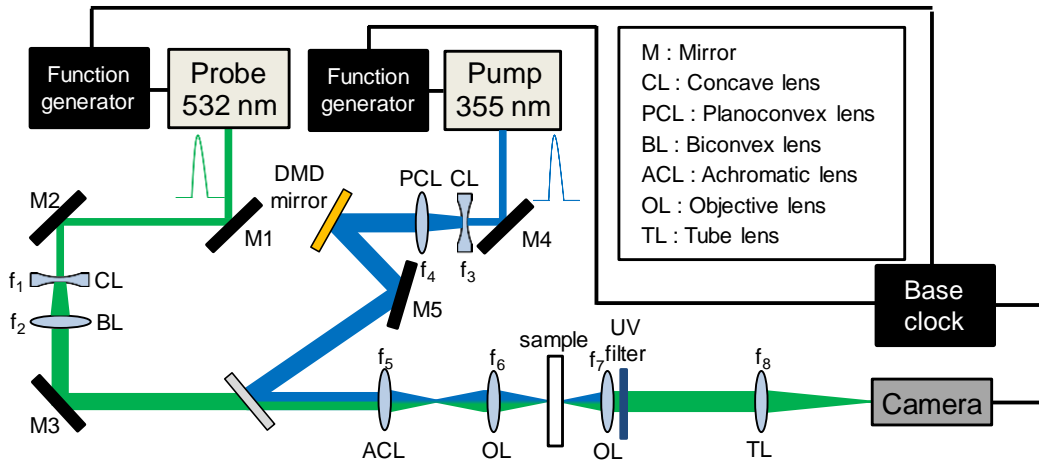


Fig. S1 The schematic overview of the optical setup of the patterned-illumination time-resolved phase microscopy (PI-PM) is shown. A pump pulse was first reflected at a digital micromirror device (DMD) mirror with an arbitrary pattern. Another probe pulse was irradiated onto the sample. For imaging purposes, an objective lens and a tube lens were used before the CMOS camera. For the pattern illumination, a DMD (Light Crafter 4500, Texas Instruments) was used. The pump light was reflected at the DMD mirror to change the intensity pattern same as the pattern on a computer. The image of the DMD mirror was relayed with a lens ( $f = 100$  mm) and an objective lens (LUCPLFLN20x, Olympus) to irradiate the same pattern reduced in size ( $1/14$ ) onto a sample. The pulsed illumination light was collimated with the pump light at the dichroic mirror and illuminated onto a sample. The transmitted light was imaged by an objective lens (LUCPLFLN20x, Olympus) and a tube lens (TTL180-A, Thorlabs). A CMOS camera (MV1-D1024E-160, Photon Focus) had a sensor area of  $10.9 \times 10.9$  mm ( $1024 \times 1024$  pixel), and the central region in the vertical direction ( $200 \times 1024$  pixel) was recorded to reduce the burden of the computer processing. The diameter of the irradiated area by the pump pulse was 0.5 mm. By varying the time delay between the pump and probe pulse, a sequence of images was stored in a computer. The time resolution was limited only by the pulse width of the pump and probe lights, 3 ns. The pump light was the third harmonics of a Nd:YAG pulse laser (pulse width: 3 ns, wavelength: 355 nm) (GAIA, Rayture Systems). The probe light was the second harmonics of an Nd:YAG pulse laser (pulse width: 3 ns, wavelength: 532 nm) (GAIA, Rayture Systems). The timing of these pulses was controlled by two function generators (WF1968, NF) triggered by a base clock (DF1906, NF). Each function generator controlled both the timing of the flash lamp and the Q-switch with a time resolution of 100 ps. The pump light intensity was 0.67 mJ/pulse, and the probe light intensity was 0.02 mJ/pulse, respectively.

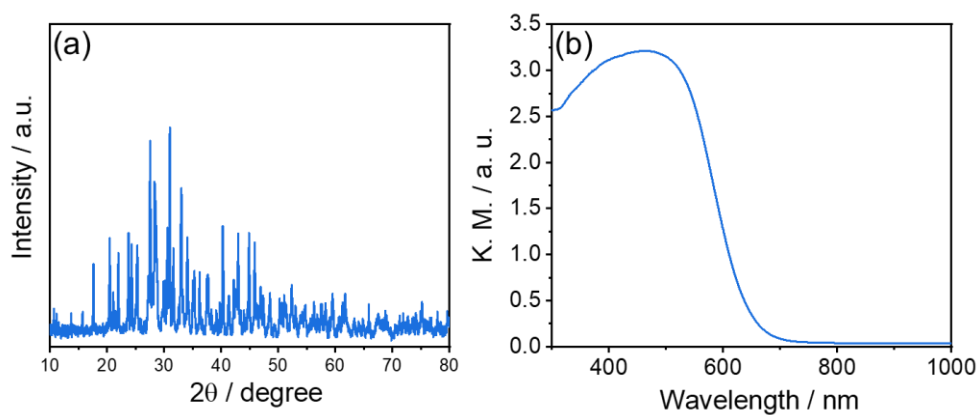


Fig.S2 (a) The XRD pattern and (b) the DRS spectrum of Ga-LTCA particulate film are shown. The film was a dense film, as explained in the experimental section.

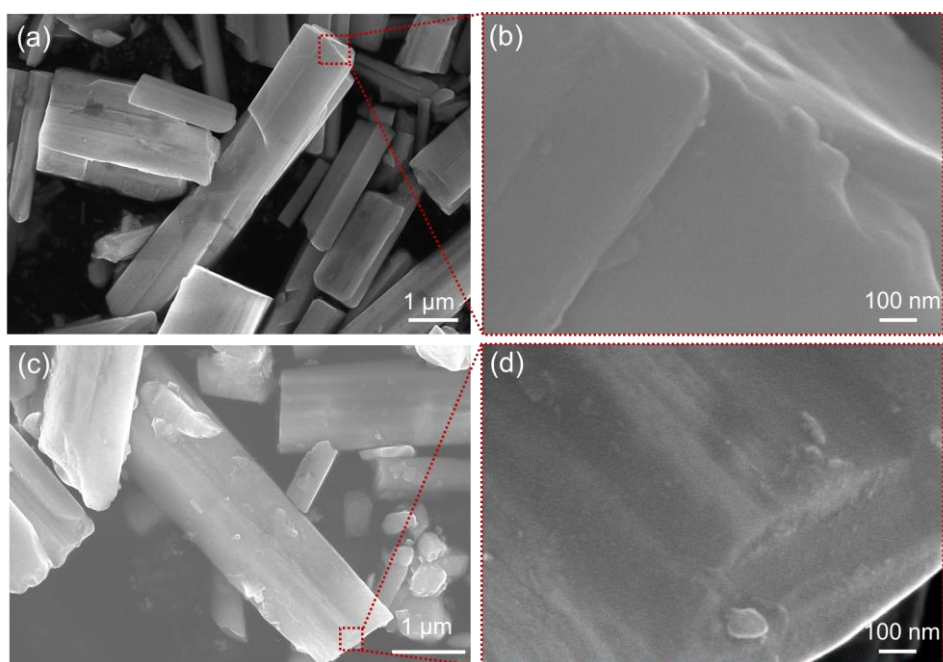


Fig. S3 HR-SEM images of (a-b) Ga-LTCA and (c-d) Rh/Ga-LTCA particles are shown.

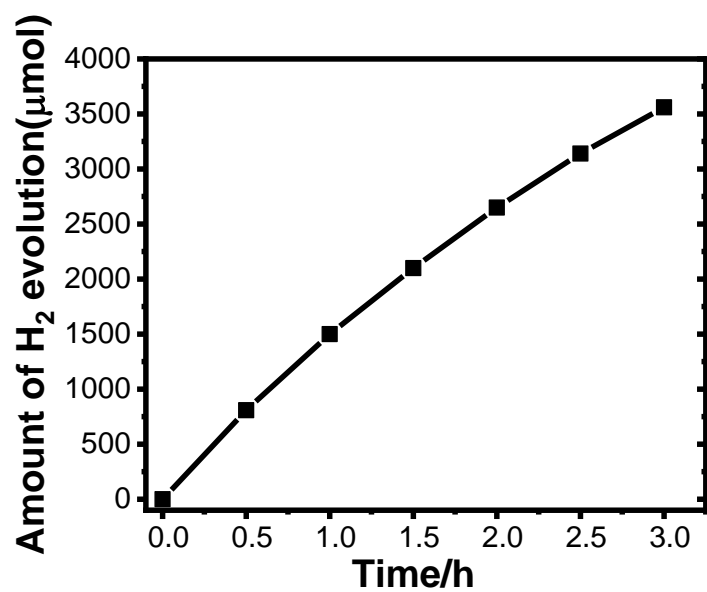


Fig. S4 The time course of the photocatalytic H<sub>2</sub> evolution by Rh/Ga-LTCA. Reaction conditions: 200 mg Rh/Ga-LTCA, 100 mL Na<sub>2</sub>S-Na<sub>2</sub>SO<sub>3</sub> (50 mM each) aqueous solution, Ar 7 kPa background pressure, 300 W Xe light source ( $\lambda > 420$  nm).

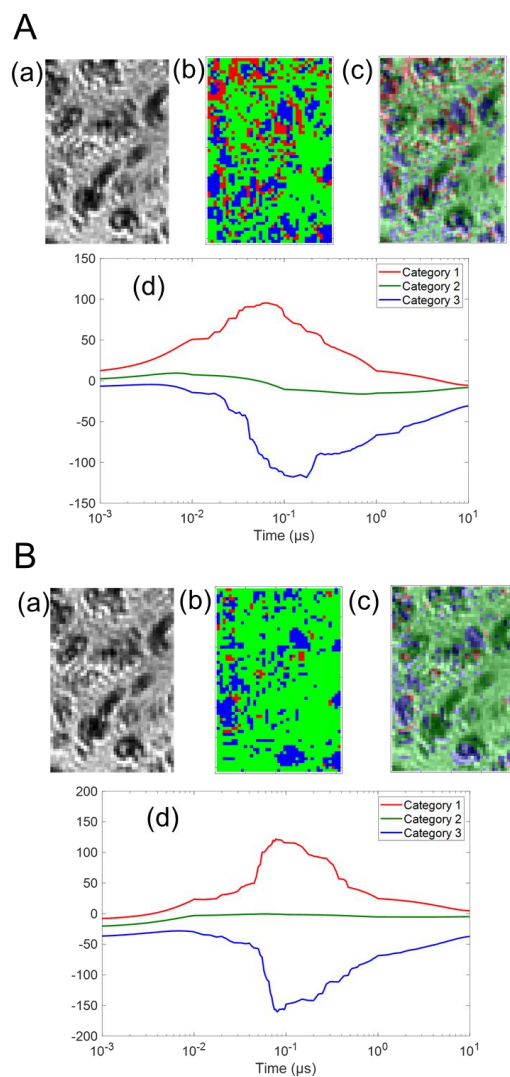


Fig. S5 The categorized maps of the charge carrier responses of Ga-LTCA in (A) ACN and (B) MeOH in region 2 of Fig. 1. (a) corresponds to a microscopic image and the corresponding categorized map is shown in (b). (c) is an image of the overlap between (a) and (b). The averaged responses for three categories are shown in (d). The ratios of Categories 1-3 of (A) Ga-LTCA in ACN was 16, 61, and 23% and that of (B) Ga-LTCA in MeOH was 3, 77, and 20%, respectively.

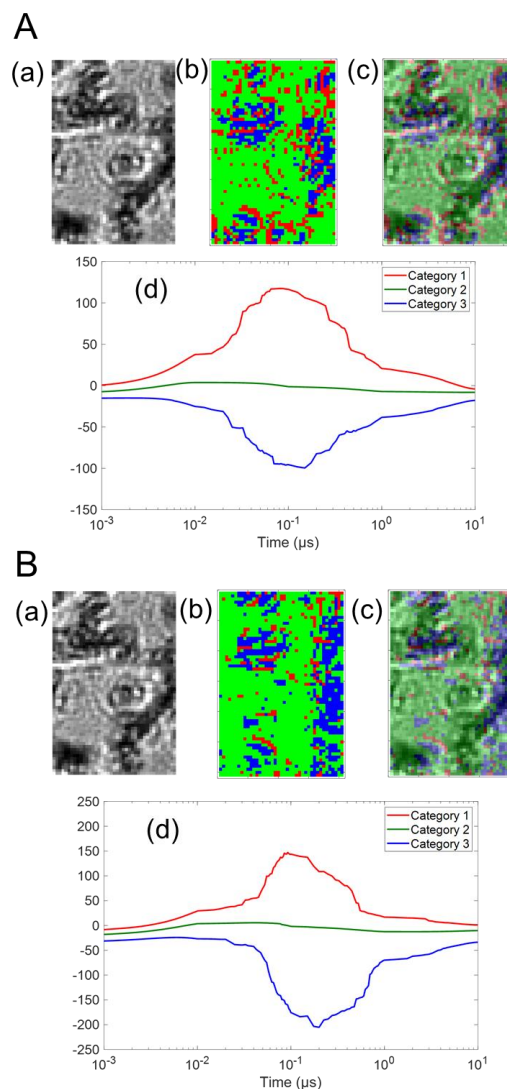


Fig. S6 The categorized maps of the charge carrier responses of Ga-LTCA in (A) ACN and (B) MeOH in region 3 of Fig. 1. (a) corresponds to a microscopic image and the corresponding categorized map is shown in (b). (c) is an image of the overlap between (a) and (b). The averaged responses for three categories are shown in (d). The ratios of Categories 1-3 of (A) Ga-LTCA in ACN was 19, 66, and 15% and that of (B) Ga-LTCA in MeOH was 8, 70, and 22%, respectively.

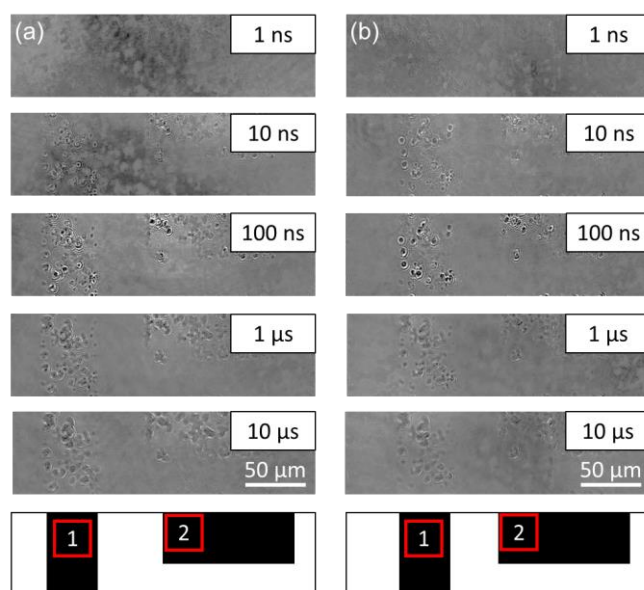


Fig. S7 The time-resolved image sequences of the refractive index change (0 ns – 10 μs) for Rh/Ga-LTCA in (a) ACN and (b) MeOH measured by the PI-PM method. The pump light patterns and the regions used for the clustering analysis were shown at the bottom, with black regions and red squares, respectively.

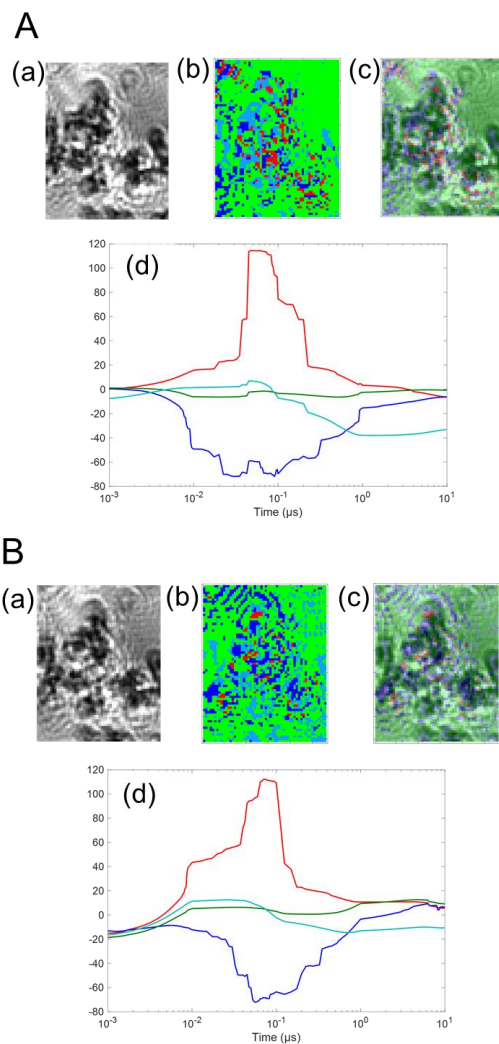


Fig. S8 The categorized maps of the charge carrier responses of Rh/Ga-LTCA in (A) ACN and (B) MeOH in region 1 of Fig. S7. (a) corresponds to a microscopic image and the corresponding categorized map is shown in (b). (c) is an image of the overlap between (a) and (b). The averaged responses for three categories are shown in (d). The ratio of category 1-4 of (A) Ga-LTCA in ACN was 6, 69, 12, and 13% and that of (B) Ga-LTCA in MeOH was 3, 62, 17, and 18%, respectively.

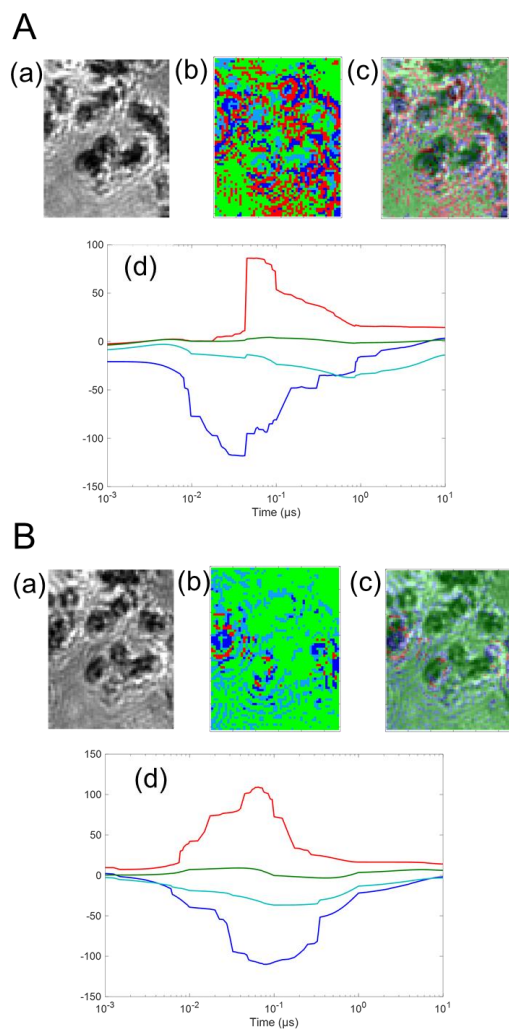


Fig. S9 The categorized maps of the charge carrier responses of Rh/Ga-LTCA in (A) ACN and (B) MeOH in region 2 of Fig. S7. (a) corresponds to a microscopic image and the corresponding categorized map is shown in (b). (c) is an image of the overlap between (a) and (b). The averaged responses for three categories are shown in (d). The ratios of Categories 1-4 of (A) Ga-LTCA in ACN was 27, 47, 15, and 12% and that of (B) Ga-LTCA in MeOH was 2, 70, 5, and 23%, respectively.

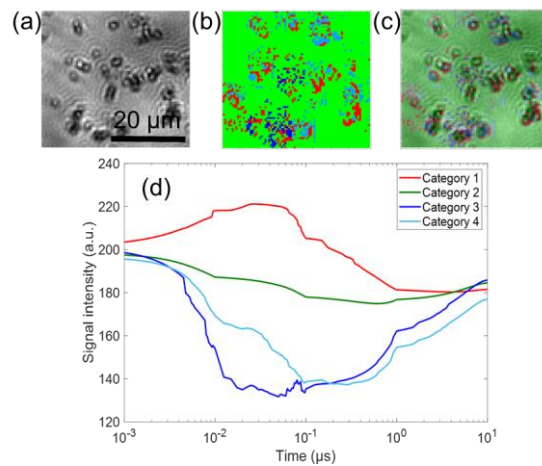


Fig. S10 The categorized mapping of the charge carrier responses of Rh/LTCA in ACN in Fig. 5(a) (region 1). (a) corresponds to a microscopic image and the corresponding categorized map is shown in (b). (c) is an image of the overlap between (a) and (b). The averaged responses for three categories are shown in (d). The ratio of Categories 1-4 was 9, 81, 3, and 7%, respectively.

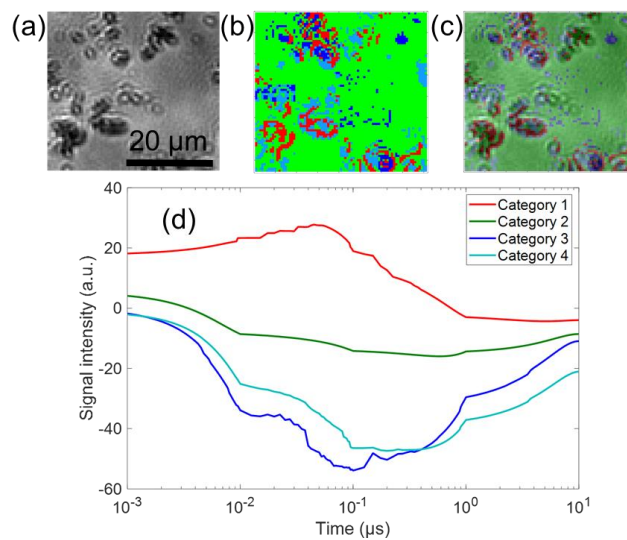


Fig. S11 The categorized mapping of the charge carrier responses of Rh/LTCA in ACN in Fig. 5(a) (region 2). (a) corresponds to a microscopic image and the corresponding categorized map is shown in (b). (c) is an image of the overlap between (a) and (b). The averaged responses for three categories are shown in (d). The ratio of Categories 1-4 was 9, 75, 5, and 11%, respectively.